ACCURATE NUMERICAL SIMULATION OF KINKING CRACKS IN COMPOSITES

S. T. Pinho*[1], B. Y. Chen[2], N. V. De Carvalho[3], P. M. Baiz[1], T. E. Tay[2]

[1]*Dept. of Aeronautics, South Kensington Campus, Imperial College London. SW7 2AZ, U.K.*
[2]*Dept. of Mech. Eng., Nat. Univ. of Singapore. 21 Lower Kent Ridge Road, Singapore 119077*
[3]*National Institute of Aerospace, NASA Langley Research Center, Hampton, USA*
* *Corresponding Author: silvestre.pinho@imperial.ac.uk*

Keywords: phantom node method, multiple cracks, matrix crack, delamination, interaction

Abstract
This paper presents a new method suitable for modelling kinking discontinuities within a finite element framework. The proposed method effectively implements local remeshing in terms of solution, but is computationally more efficient than remeshing; it can be readily implemented in relatively closed FE codes; and it allows (sub-)elements near a crack tip to readily share information. The finite element architecture of the new method is similar to that of the phantom node method. Validation examples show that the proposed method can predict stress intensity factors and crack propagation accurately. An application example shows that the proposed method can predict the transition from matrix cracking to delamination in cross-ply composite laminates by accurately representing T-shaped cracks inside an element.

1. Introduction

This paper focuses on the accurate numerical representation of complex networks of evolving discontinuities in solids, with particular emphasis on cracks. The limitation of the standard finite element method (FEM) in approximating discontinuous solutions has motivated the development of re-meshing [1], smeared crack models [2, 3], the eXtended Finite Element Method (XFEM) [4, 5, 6] and the Phantom Node Method (PNM) [7].

We propose a new method which has some similarities to the PNM, but crucially: (i) does not introduce an error on the crack geometry when mapping to natural coordinates; (ii) does not require numerical integration over *only part* of a domain; (iii) can incorporate weak discontinuities and cohesive cracks more readily; (iv) is ideally suited for the representation of multiple and complex networks of (weak, strong and cohesive) discontinuities; (v) leads to the same solution as a finite element mesh where the discontinuity is represented explicitly; and (vi) is conceptually simpler than the PNM.

2. Theory

The proposed floating node method is described in detail elsewhere [8, 9]. Fig. 1 compares schematically the method to the well known Phantom Node Method. Additionally, Fig. 1a can

also be interpreted as an automated form of local remeshing. Fig. 2 shows examples of different types of discontinuities that can be represented with the method. The method can be used with cohesive elements and with VCCT for crack propagation [8, 9].

3. Validation

3.1. Convergence and accuracy

We compare the mesh convergence of the PNM and FNM in the evaluation of stress intensity factors (SIF) for an edge crack propagating in mode I (Fig. 3a). The numerical evaluations for the FNM are performed with VCCT, and for PNM with VCCT as implemented in the commercial software Abaqus [10]. Further details are given in [8, 9]. The results are summarized in Fig. 3b. The FNM can be seen to converge monotonically and more rapidly than the PNM used for comparison.

We now evaluate the stress intensity factors (SIF) for a centre slant crack (Fig. 4a) obtained by the FNM against the corresponding analytical solutions [11] in mode I (K_{I}) and mode II (K_{II}), for different orientations θ of the crack. The numerical evaluations for the FNM are performed with VCCT. For FNM with VCCT, when the crack separates the original element domain into a triangle and a pentagon, both the partitions shown in Fig. **??** and that shown in Fig. **??** are employed. Further model details are given in [8, 9]. The results are summarized in Fig. 4b. The data-points labelled 'Int. 1' are obtained with FNM-VCCT using the partition in Fig. **??**, and the data-points labelled 'Int. 2' are obtained with FNM-VCCT using the partition in Fig. **??**.

3.2. Crack propagation

A double cantelever beam (DCB) test is used to simulate a propagating crack for a case in which the analytical solution (using corrected beam theory [12]) is known. Further model details are given in [8, 9]. The cohesive zone approach with a standard bi-linear law and a stress-based criterion is employed to determine the initiation and propagation of a crack.

This case is analysed with both the FNM and the PNM (the latter implemented in the commercial software Abaqus [10]). For the FNM, the transition element shown in Fig. **??** is employed for the element in front of the crack tip. The results are shown in Fig. 5b.

4. Application: modelling of the growth of matrix crack density in a cross-ply laminate

In this section, we analyse the problem of interaction between matrix cracks and delamination on a cross-ply $[0_2/90_4]_{\mathrm{S}}$ laminate of toughened glass/epoxy, tested in tension by Joffe and Varna [13]. In this problem, correctly capturing the matrix crack/delamination interaction mechanism is important for the accurate prediction of matrix crack saturation and consequent transition to delamination.

Fang et al. [14] (see Fig. 6a) showed that using non-matching meshes at a crack intersection (e.g. using the PNM for the 90° matrix cracks in the 90° ply and cohesive elements at the interface for the delamination) leads to an inaccurate representation of the displacement jump (and hence of the cohesive traction) at the interface. Capturing correctly the displacement jump

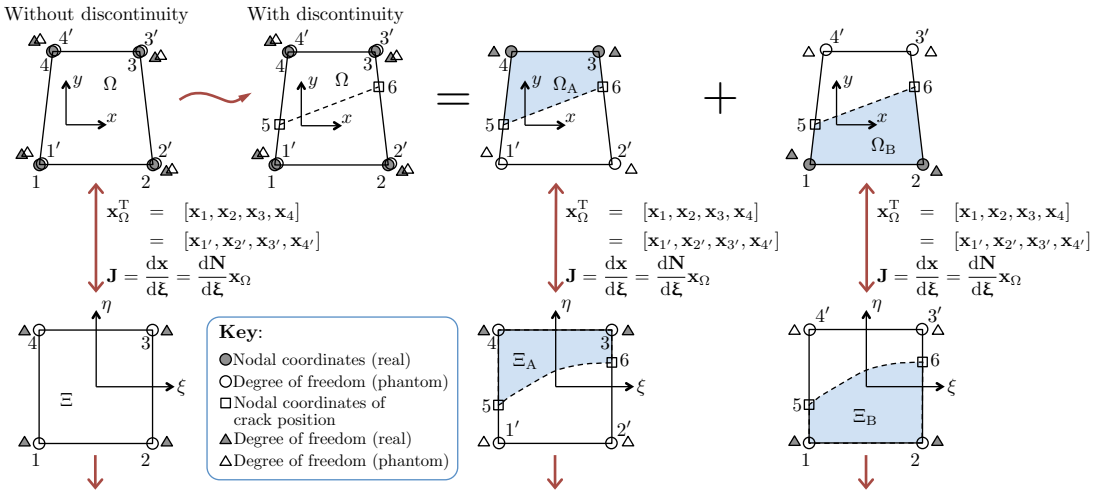

$$\mathbf{x}_\Omega^{\mathrm{T}} = [\mathbf{x}_1, \mathbf{x}_2, \mathbf{x}_3, \mathbf{x}_4] = [\mathbf{x}_{1'}, \mathbf{x}_{2'}, \mathbf{x}_{3'}, \mathbf{x}_{4'}]$$

$$\mathbf{J} = \frac{\mathrm{d}\mathbf{x}}{\mathrm{d}\boldsymbol{\xi}} = \frac{\mathrm{d}\mathbf{N}}{\mathrm{d}\boldsymbol{\xi}}\mathbf{x}_\Omega$$

$$\mathbf{q}^{\mathrm{T}} = [\mathbf{q}_1, \mathbf{q}_2, \mathbf{q}_3, \mathbf{q}_4]$$

$$\mathbf{u} = \mathbf{N}\mathbf{q}$$

$$\boldsymbol{\epsilon} = \mathcal{L}_{\mathbf{x}}(\mathbf{u}) = \mathcal{L}_{\boldsymbol{\xi}}(\mathbf{N})\,\mathbf{J}^{-1}\mathbf{q}$$

$$\mathbf{K} = \int_\Xi \mathbf{B}^{\mathrm{T}}\mathbf{D}\mathbf{B}\det(\mathbf{J})\,\mathrm{d}\Xi$$

$$\mathbf{Q} = \int_\Xi \mathbf{N}^{\mathrm{T}}\mathbf{f}\det(\mathbf{J})\,\mathrm{d}\Xi + \int_{\Gamma_\Xi} \mathbf{N}^{\mathrm{T}}\mathbf{t}\det(\mathbf{J})\,\mathrm{d}\Gamma_\Xi$$

$$\mathbf{K}\mathbf{q} = \mathbf{Q}$$

$$\mathbf{x}_\Omega^{\mathrm{T}} = [\mathbf{x}_1, \mathbf{x}_2, \mathbf{x}_3, \mathbf{x}_4] = [\mathbf{x}_{1'}, \mathbf{x}_{2'}, \mathbf{x}_{3'}, \mathbf{x}_{4'}]$$

$$\mathbf{J} = \frac{\mathrm{d}\mathbf{x}}{\mathrm{d}\boldsymbol{\xi}} = \frac{\mathrm{d}\mathbf{N}}{\mathrm{d}\boldsymbol{\xi}}\mathbf{x}_\Omega$$

$$\mathbf{q}_{\mathrm{A}}^{\mathrm{T}} = [\mathbf{q}_{1'}, \mathbf{q}_{2'}, \mathbf{q}_3, \mathbf{q}_4]$$

$$\mathbf{u}_{\mathrm{A}} = \mathbf{N}\mathbf{q}_{\mathrm{A}}$$

$$\boldsymbol{\epsilon}_{\mathrm{A}} = \mathcal{L}_{\mathbf{x}}(\mathbf{u}_{\mathrm{A}}) = \mathcal{L}_{\boldsymbol{\xi}}(\mathbf{N})\,\mathbf{J}^{-1}\mathbf{q}_{\mathrm{A}}$$

$$\mathbf{K}_{\mathrm{A}} = \int_{\Xi_{\mathrm{A}}} \mathbf{B}^{\mathrm{T}}\mathbf{D}\mathbf{B}\det(\mathbf{J})\,\mathrm{d}\Xi$$

$$\mathbf{Q}_{\mathrm{A}} = \int_{\Xi_{\mathrm{A}}} \mathbf{N}^{\mathrm{T}}\mathbf{f}\det(\mathbf{J})\,\mathrm{d}\Xi + \int_{\Gamma_{\Xi_{\mathrm{A}}}} \mathbf{N}^{\mathrm{T}}\mathbf{t}\det(\mathbf{J})\,\mathrm{d}\Gamma_\Xi$$

$$\mathbf{K}_{\mathrm{A}}\mathbf{q}_{\mathrm{A}} = \mathbf{Q}_{\mathrm{A}}$$

$$\mathbf{x}_\Omega^{\mathrm{T}} = [\mathbf{x}_1, \mathbf{x}_2, \mathbf{x}_3, \mathbf{x}_4] = [\mathbf{x}_{1'}, \mathbf{x}_{2'}, \mathbf{x}_{3'}, \mathbf{x}_{4'}]$$

$$\mathbf{J} = \frac{\mathrm{d}\mathbf{x}}{\mathrm{d}\boldsymbol{\xi}} = \frac{\mathrm{d}\mathbf{N}}{\mathrm{d}\boldsymbol{\xi}}\mathbf{x}_\Omega$$

$$\mathbf{q}_{\mathrm{B}}^{\mathrm{T}} = [\mathbf{q}_1, \mathbf{q}_2, \mathbf{q}_{3'}, \mathbf{q}_{4'}]$$

$$\mathbf{u}_{\mathrm{B}} = \mathbf{N}\mathbf{q}_{\mathrm{B}}$$

$$\boldsymbol{\epsilon}_{\mathrm{B}} = \mathcal{L}_{\mathbf{x}}(\mathbf{u}_{\mathrm{B}}) = \mathcal{L}_{\boldsymbol{\xi}}(\mathbf{N})\,\mathbf{J}^{-1}\mathbf{q}_{\mathrm{B}}$$

$$\mathbf{K}_{\mathrm{B}} = \int_{\Xi_{\mathrm{B}}} \mathbf{B}^{\mathrm{T}}\mathbf{D}\mathbf{B}\det(\mathbf{J})\,\mathrm{d}\Xi$$

$$\mathbf{Q}_{\mathrm{B}} = \int_{\Xi_{\mathrm{B}}} \mathbf{N}^{\mathrm{T}}\mathbf{f}\det(\mathbf{J})\,\mathrm{d}\Xi + \int_{\Gamma_{\Xi_{\mathrm{B}}}} \mathbf{N}^{\mathrm{T}}\mathbf{t}\det(\mathbf{J})\,\mathrm{d}\Gamma_\Xi$$

$$\mathbf{K}_{\mathrm{B}}\mathbf{q}_{\mathrm{B}} = \mathbf{Q}_{\mathrm{B}}$$

(a) Phantom Node Method

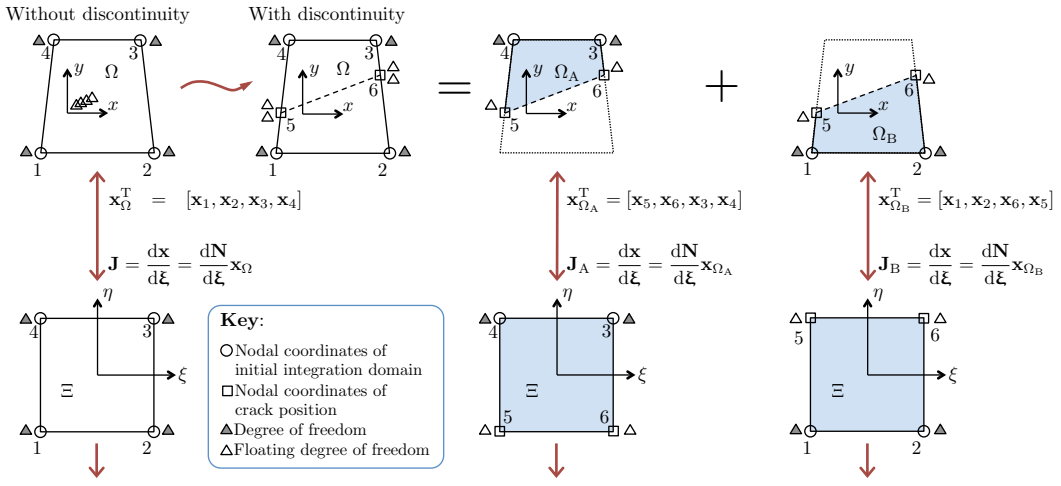

$$\mathbf{x}_\Omega^{\mathrm{T}} = [\mathbf{x}_1, \mathbf{x}_2, \mathbf{x}_3, \mathbf{x}_4]$$

$$\mathbf{J} = \frac{\mathrm{d}\mathbf{x}}{\mathrm{d}\boldsymbol{\xi}} = \frac{\mathrm{d}\mathbf{N}}{\mathrm{d}\boldsymbol{\xi}}\mathbf{x}_\Omega$$

$$\mathbf{q}^{\mathrm{T}} = [\mathbf{q}_1, \mathbf{q}_2, \mathbf{q}_3, \mathbf{q}_4]$$

$$\mathbf{u} = \mathbf{N}\mathbf{q}$$

$$\boldsymbol{\epsilon} = \mathcal{L}_{\mathbf{x}}(\mathbf{u}) = \mathcal{L}_{\boldsymbol{\xi}}(\mathbf{N})\,\mathbf{J}^{-1}\mathbf{q}$$

$$\mathbf{K} = \int_\Xi \mathbf{B}^{\mathrm{T}}\mathbf{D}\mathbf{B}\det(\mathbf{J})\,\mathrm{d}\Xi$$

$$\mathbf{Q} = \int_\Xi \mathbf{N}^{\mathrm{T}}\mathbf{f}\det(\mathbf{J})\,\mathrm{d}\Xi + \int_{\Gamma_\Xi} \mathbf{N}^{\mathrm{T}}\mathbf{t}\det(\mathbf{J})\,\mathrm{d}\Gamma_\Xi$$

$$\mathbf{K}\mathbf{q} = \mathbf{Q}$$

$$\mathbf{x}_{\Omega_{\mathrm{A}}}^{\mathrm{T}} = [\mathbf{x}_5, \mathbf{x}_6, \mathbf{x}_3, \mathbf{x}_4]$$

$$\mathbf{J}_{\mathrm{A}} = \frac{\mathrm{d}\mathbf{x}}{\mathrm{d}\boldsymbol{\xi}} = \frac{\mathrm{d}\mathbf{N}}{\mathrm{d}\boldsymbol{\xi}}\mathbf{x}_{\Omega_{\mathrm{A}}}$$

$$\mathbf{q}_{\mathrm{A}}^{\mathrm{T}} = [\mathbf{q}_5, \mathbf{q}_6, \mathbf{q}_3, \mathbf{q}_4]$$

$$\mathbf{u}_{\mathrm{A}} = \mathbf{N}\mathbf{q}_{\mathrm{A}}$$

$$\boldsymbol{\epsilon}_{\mathrm{A}} = \mathcal{L}_{\mathbf{x}}(\mathbf{u}_{\mathrm{A}}) = \mathcal{L}_{\boldsymbol{\xi}}(\mathbf{N})\,\mathbf{J}_{\mathrm{A}}^{-1}\mathbf{q}_{\mathrm{A}}$$

$$\mathbf{K}_{\mathrm{A}} = \int_\Xi \mathbf{B}_{\mathrm{A}}^{\mathrm{T}}\mathbf{D}\mathbf{B}_{\mathrm{A}}\det(\mathbf{J}_{\mathrm{A}})\,\mathrm{d}\Xi$$

$$\mathbf{Q}_{\mathrm{A}} = \int_\Xi \mathbf{N}^{\mathrm{T}}\mathbf{f}\det(\mathbf{J}_{\mathrm{A}})\,\mathrm{d}\Xi + \int_{\Gamma_\Xi} \mathbf{N}^{\mathrm{T}}\mathbf{t}\det(\mathbf{J}_{\mathrm{A}})\,\mathrm{d}\Gamma_\Xi$$

$$\mathbf{K}_{\mathrm{A}}\mathbf{q}_{\mathrm{A}} = \mathbf{Q}_{\mathrm{A}}$$

$$\mathbf{x}_{\Omega_{\mathrm{B}}}^{\mathrm{T}} = [\mathbf{x}_1, \mathbf{x}_2, \mathbf{x}_6, \mathbf{x}_5]$$

$$\mathbf{J}_{\mathrm{B}} = \frac{\mathrm{d}\mathbf{x}}{\mathrm{d}\boldsymbol{\xi}} = \frac{\mathrm{d}\mathbf{N}}{\mathrm{d}\boldsymbol{\xi}}\mathbf{x}_{\Omega_{\mathrm{B}}}$$

$$\mathbf{q}_{\mathrm{B}}^{\mathrm{T}} = [\mathbf{q}_1, \mathbf{q}_2, \mathbf{q}_{6'}, \mathbf{q}_{5'}]$$

$$\mathbf{u}_{\mathrm{B}} = \mathbf{N}\mathbf{q}_{\mathrm{B}}$$

$$\boldsymbol{\epsilon}_{\mathrm{B}} = \mathcal{L}_{\mathbf{x}}(\mathbf{u}_{\mathrm{B}}) = \mathcal{L}_{\boldsymbol{\xi}}(\mathbf{N})\,\mathbf{J}_{\mathrm{B}}^{-1}\mathbf{q}_{\mathrm{B}}$$

$$\mathbf{K}_{\mathrm{B}} = \int_\Xi \mathbf{B}_{\mathrm{B}}^{\mathrm{T}}\mathbf{D}\mathbf{B}_{\mathrm{B}}\det(\mathbf{J}_{\mathrm{B}})\,\mathrm{d}\Xi$$

$$\mathbf{Q}_{\mathrm{B}} = \int_\Xi \mathbf{N}^{\mathrm{T}}\mathbf{f}\det(\mathbf{J}_{\mathrm{B}})\,\mathrm{d}\Xi + \int_{\Gamma_\Xi} \mathbf{N}^{\mathrm{T}}\mathbf{t}\det(\mathbf{J}_{\mathrm{B}})\,\mathrm{d}\Gamma_\Xi$$

$$\mathbf{K}_{\mathrm{B}}\mathbf{q}_{\mathrm{B}} = \mathbf{Q}_{\mathrm{B}}$$

(b) Floating Node Method

Figure 1: Comparison between the Phantom Node Method and the Floating Node Method.

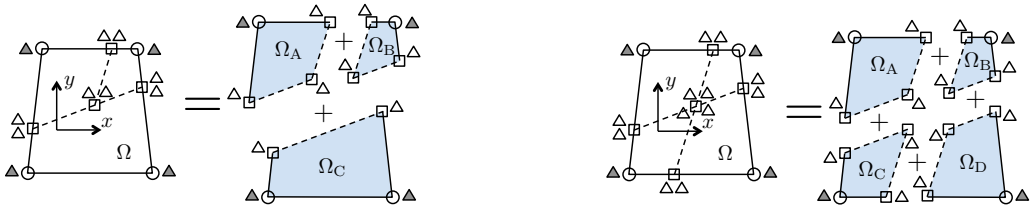

(a) T-crack (b) Intersecting cracks

Figure 2: Examples of different discontinuities that can be modelled by the Floating Node Method (see key in Fig. 1b).

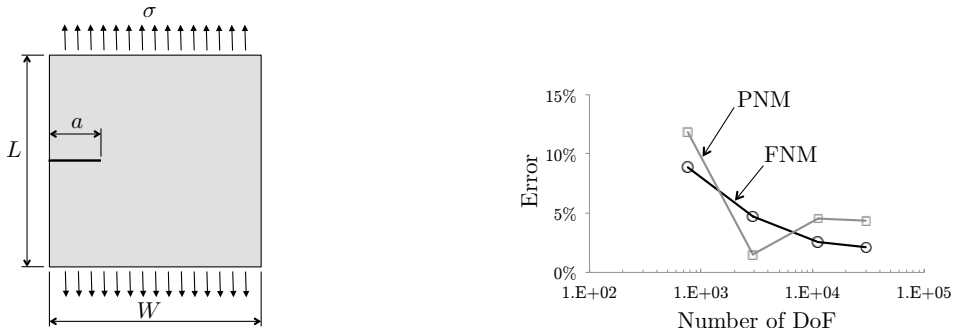

(a) Edge crack model (b) Mesh convergence of SIF

Figure 3: For this edge crack model, the FNM converges monotonically, unlike the PNM.

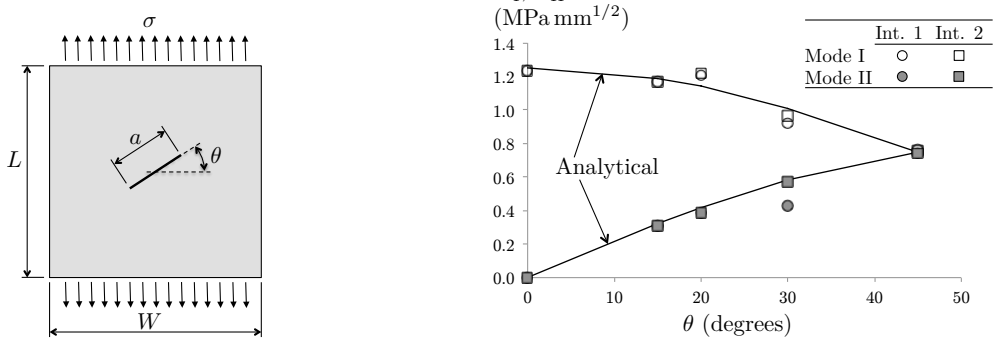

(a) Slanted crack model (b) SIF evaluations for different angles θ

Figure 4: The FNM captures the SIF well in modes I and II for different angles θ.

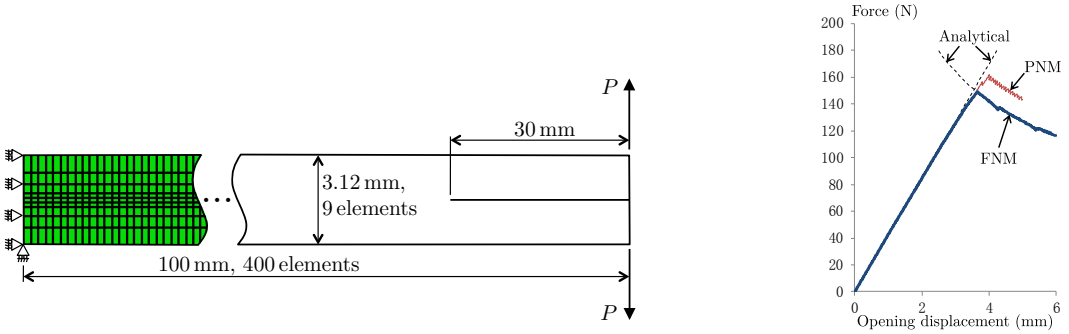

(a) DCB model

(b) Predictions

Figure 5: DCB validation case, showing that, for the same mesh seeding, the FNM predicts accuratelly the force (P) vs. displacement curve while the PNM overpredicts the force.

requires further DoF at the intersection between cracks (Fig. 6b); the FNM method is particularly well suited to model intersecting cracks, capturing correctly the displacement jump at the interface.

Based on the FNM, an element specifically designed for cross-ply laminates is formed with both real nodes and floating nodes, as shown in Fig. 6c. It makes use of the known position of the interface, so that the interface is not seeded with real nodes (Fig. 6d); instead, it is represented by cohesive elements formed with floating nodes. In this way, minimum seeding is required during preprocessing.

Since the loading is uniform in tension, a 10% reduction on transverse tensile strength and mode I critical energy release rate is introduced in the element at the centre so as to initiate failure at the centre of the model. The model, Fig. 7a, represents half of the laminate, with symmetric boundary conditions applied on the bottom surface of the 90° plies. Further model details are given in [8, 9].

Figs. 7b and 7c show the failure pattern predictions for the laminate when using the FNM element from Figs. 6c and 6d. To demonstrate how crucial it is to have matching meshes at the crack intersections, a second model was created, differing only in that only one cohesive sub-element is used to model the delamination in each FNM element (as in Fig. 6a), rather than two. This second model corresponds very closely to a model in which matrix cracks in the 90° ply are modelled with the PNM and the delamination is modelled independently using cohesive elements. The resulting crack pattern, at the same level of strain as in Figs. 7b and 7c, is shown in Figs. 7d and 7e. The second model predicts significantly less delamination than the FNM model. The simulation shows that delamination does not start from the element containing the matrix crack; instead, it occurs firstly in the elements next to the cracked element. This non-physical sequence of delamination propagation is expected in the formulation of the non-matching meshes (Fig. 6a).

Fig. 8 shows the crack density vs. applied strain predictions. While both models are able to capture the growth of crack density with applied strain, only the first model (with matching mesh at the crack intersections) is able to predict saturation accurately; the second model continues to predict an increase in crack density, albeit at a lower growth rate, after saturation should

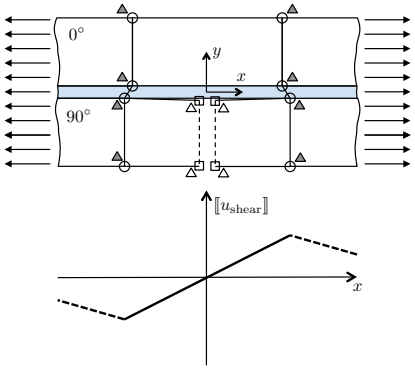

(a) Non-matching meshes at intersection [14].

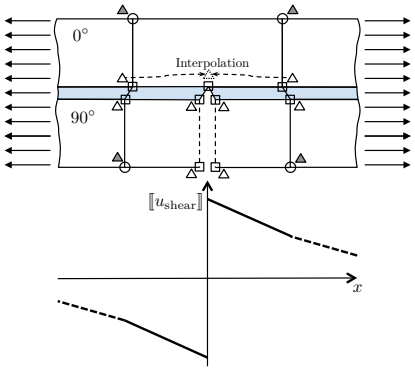

(b) FNM element with intersecting cracks [14].

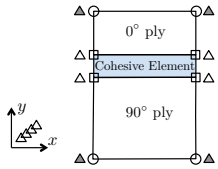

(c) FNM element before matrix cracking.

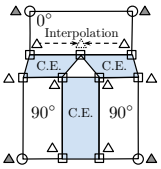

(d) FNM element after matrix cracking.

Figure 6: Modelling the intersection between matrix cracks and delamination with non-matching meshes fails to capture the displacement jump; the FNM can address this.

have occurred. This example thus demonstrates the capability of using the FNM to construct elements for the modelling of specific geometries and complex crack networks.

5. Conclusion

This paper proposes a floating node method which can be implemented in existing finite element packages. The paper demonstrates that the floating node method has the following advantages over alternative methods, in particular the phantom node method: (i) it does not introduce an error on the crack geometry when mapping from physical to natural coordinates; (ii) the integration is simple, as it does not require numerical integration over *only part* of a domain; (iii) it leads to the same solution as a finite element mesh where the discontinuity is represented explicitly; (iv) it can incorporate weak discontinuities and cohesive cracks readily; (v) it can be readily combined with VCCT; (vi) it provides accurate predictions for stress intensity factors under generic mode ratios; (vii) it is ideally suited for the representation of multiple and complex networks of (weak, strong and cohesive) discontinuities; and (viii) it can successfully predict certain interactions between matrix cracking and delamination.

Acknowledgement

The second author acknowledges the scholarship from National University of Singapore.

References

[1] H. Azadi and A. R. Khoei. Numerical simulation of multiple crack growth in brittle materials with adaptive remeshing. *International Journal for Numerical Methods in Engineering*, 85:1017–1048, 2011.

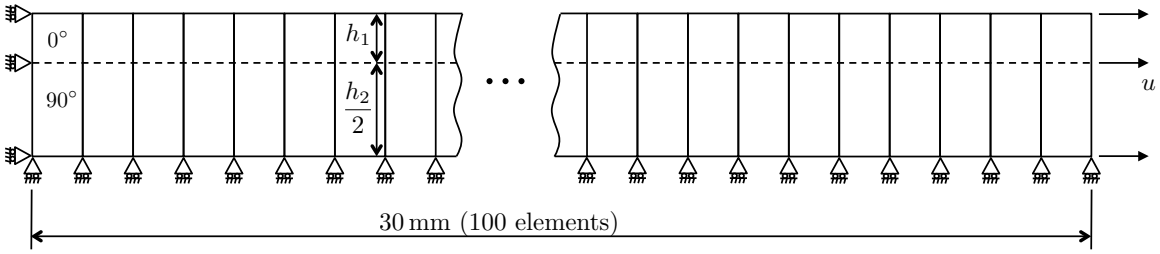

(a) FNM model. Note that there is only one floating node element along the height (see Figs. 6c and 6d).

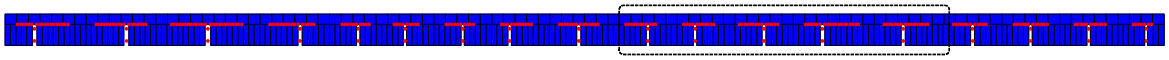

(b) Accurate modelling of the transition from matrix cracking to delamination when using the FNM element from Figs. 6c and 6d.

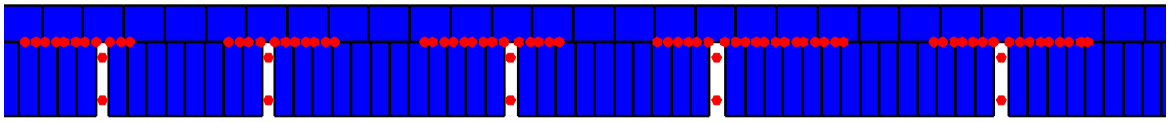

(c) Zoom of FNM mesh in Fig. 7b.

(d) Model with non-matching mesh at the intersection, showing that some transition to delamination is not correctly captured.

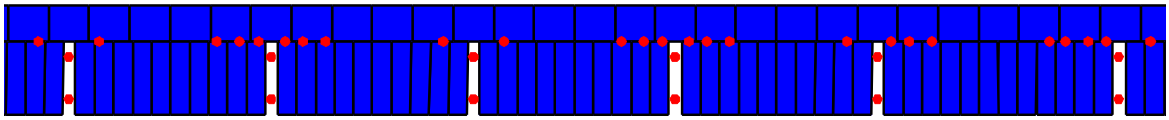

(e) Zoom of non-matching mesh in Fig. 7d.

Figure 7: Modelling the transition from matrix cracking to delamination in a cross-ply composite specimen. The red dots indicate failure at the corresponding integration points.

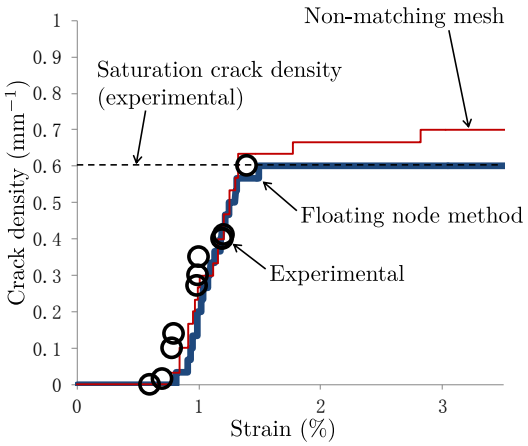

Figure 8: The saturation crack density is correctly captured using the FNM element from Figs. 6c and 6d. Non-matching mesh results in over-prediction of this density. Experimental data is from Joffe and Varna [13].

[2] Z. P. Bažant and B.H. Oh. Crack band theory for fracture of concrete. *Matériaux et Construction*, 16(3):155–177, 1983.

[3] S. T. Pinho, L. Iannucci, and P. Robinson. Physically based failure models and criteria for laminated fibre-reinforced composites with emphasis on fibre kinking. Part II: FE implementation. *Composites Part A-Applied Science and Manufacturing*, 37(5):766–777, 2006.

[4] N. Moës, J. Dolbow, and T. Belytschko. A finite element method for crack growth without remeshing. *International Journal for Numerical Methods in Engineering*, 46(1):131–150, 1999.

[5] Joris J. C. Remmers, Rene de Borst, and Alan Needleman. The simulation of dynamic crack propagation using the cohesive segments method. *Journal of the Mechanics and Physics of Solids*, 56(1):70–92, 2008.

[6] Luiz F. Kawashita, Alexandre Bedos, and Stephen R. Hallett. Modelling Mesh Independent Transverse Cracks in Laminated Composites with a Simplified Cohesive Segment Method. *Computers, Materials & Continua*, 32(2):133–158, 2012.

[7] Pedro M. A. Areias, J. H. Song, and Ted Belytschko. Analysis of fracture in thin shells by overlapping paired elements. *Computer Methods in Applied Mechanics and Engineering*, 195(41-43):5343–5360, 2006.

[8] S. T. Pinho, B. Y. Chen, P. M. Baiz, N. V. De Carvalho, and T. E. Tay. A floating node method for modeling multiple discontinuities within an element. In *19th International Conference on Composite Materials*, Montreal, Canada, 28 July - 2 August 2013.

[9] S. T. Pinho, B. Y. Chen, P. M. Baiz, N. V. De Carvalho, and T. E. Tay. A floating node method for modeling multiple discontinuities within an element. *Engineering Fracture Mechanics; Accepted for publication*, 2014.

[10] Dassault Systèmes Simulia Corp. *Abaqus 6.10 documentation*. Dassault Systèmes, Providence, RI, USA, 2010.

[11] H. Tada, P. C. Paris, and G. R. Irwin. *The stress analysis of cracks handbook*. Second edition, Paris Productions Incorporated (and Del Research Corporation), 226 Woodbourne Dr. St. Louis, Missouri. 1985.

[12] James R. Reeder, Kevin Demarco, and Karen S. Whitley. The use of doubler reinforcement in delamination toughness testing. *Composites Part A: Applied Science and Manufacturing*, 35(11):1337 – 1344, 2004.

[13] R. Joffe and J. Varna. Analytical modeling of stiffness reduction in symmetric and balanced laminates due to cracks in 90° layers. *Composites Science and Technology*, 59(11):1641 – 1652, 1999.

[14] X. J. Fang, Q. D. Yang, B. N. Cox, and Z. Q. Zhou. An augmented cohesive zone element for arbitrary crack coalescence and bifurcation in heterogeneous materials. *International Journal for Numerical Methods in Engineering*, 88:841–861, 2011.